Resonance-enhanced isotope-selective photoionization of YbI for ion trap loading

M. Johanning · A. Braun · D. Eiteneuer · C. Paape · C. Balzer · W. Neuhauser · C. Wunderlich

Abstract Neutral ytterbium (YbI) and singly ionized ytterbium (YbII) are widely used in experiments in quantum optics, metrology, and quantum information science. We report on the investigation of isotope-selective two-photon ionization of YbI that allows for efficient loading of ion traps with YbII. Results are presented on two-color (399 nm and 369 nm) and single-color (399 nm) photoionization and their efficiency is compared to electron impact ionization. Nearly deterministic loading of a desired number of YbII ions into a linear Paul trap is demonstrated. First results have been presented in the context of quantum information (Balzer et al. in Phys. Rev. A 73:041407(R), 2006), and the present paper is intended to give a detailed description and understanding of the photoionization and ion trap loading processes. Furthermore, we provide useful technical details of the production and characterization of suitable atomic ovens.

1 Introduction

Atomic and singly ionized ytterbium is the element of choice in numerous experiments in atomic physics and quantum optics. Trapping and laser cooling of ^{171}Yb$^+$ in Paul traps was initially motivated by its potential use as a frequency standard in the microwave or optical regime [2–10]. In addition, this element is now employed by an increasing number of research groups for implementing experiments related to quantum information science (e.g. [1, 11–16]). In [17], loading of shallow ion traps was demonstrated from a cold sample of neutral ytterbium, using the same photoionization process which is investigated here, which in those experiments was provided by the combined cooling light for the neutral atoms and ions. Neutral Yb is used, for instance, in Bose–Einstein condensation [18], in photoassociation [19], or for experiments aiming at the measurement of parity violation in atoms [20].

An important step in trapping ions is the ionization process. For almost 25 years since the first successful trapping and laser cooling of atomic ions [21, 22], electron impact ionization was the process of choice. In recent years, photoionization has begun to establish itself as an attractive ionization process for different elements, as it offers distinct advantages over electron impact ionization [1, 23–28]. First, it is highly efficient in comparison with electron impact ionization, typically yielding loading rates that are several orders of magnitude higher. This allows the neutral atom flux to be reduced considerably, thus avoiding contamination by deposition of atoms on trap electrodes or other, isolating trap components. Second, the electron bombardment introduces excess charge into the trap volume and on trap components that disturbs the trapping potential. This effect, too, is avoided when using photoionization. And, third, by employing a resonantly enhanced process, photoionization can be made isotope selective in contrast to indiscriminate trap loading with the electron impact method. Thus, the need for isotope-enriched samples, often a prerequisite for experiments with isotopically pure ionic crystals, is eliminated.

In this article we present an investigation of photoionization of atomic ytterbium, with particular attention to its use as a loading process for ion traps. A further advantage of the

M. Johanning · A. Braun · D. Eiteneuer · C. Balzer · C. Wunderlich (✉)
Department Physik, Naturwissenchaftlich-Technische Fakultät, Universität Siegen, 57068 Siegen, Germany
e-mail: wunderlich@physik.uni-siegen.de

C. Paape · W. Neuhauser
Institut für Laser-Physik, Universität Hamburg, Luruper Chaussee 149, 22761 Hamburg, Germany

Fig. 1 Partial energy level scheme of YbI. Two resonances convenient for laser excitation and subsequent photoionization are indicated by arrows

Fig. 2 Two-photon ionization of YbI via the $^1P_1$ state
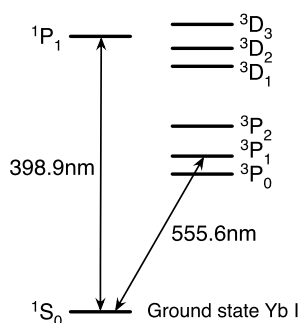
scheme presented here is the need for only one light source at a convenient wavelength near 399 nm that is reasonably close to the now established industrial standard at 405 nm for laser diodes, making access to inexpensive laser light sources more likely. Recent progress in laser diode production processes, however, makes outliers, which deliver the desired wavelength, less probable and makes it necessary to use cooled laser diodes [14].

In Sect. 2 we report on laser spectroscopy of the $^1S_0$–$^1P_1$ resonance near 399 nm in YbI with the hyperfine structure resolved. Resonance fluorescence spectra are recorded employing a collimated thermal atomic beam emerging from an Yb oven. We present a simplified model of this Yb oven in Sect. 3 that predicts measured oven temperatures satisfyingly and agrees with density and flux measurements presented in Sect. 4. Resonance-enhanced photoionization of YbI using an additional light field near 369 nm is then reported in Sect. 5 while in Sect. 6 it is shown that the light field near 399 nm alone may ionize YbI in the presence of the rf field used for ion trapping. Section 7 concludes this article.

2 Laser spectroscopy of neutral Yb

Photoionization of Yb by one photon would require radiation with wavenumber larger than 50443 cm^{-1} [29] corresponding to a wavelength below 200 nm in the vacuum-UV range. Generating and guiding radiation in this wavelength regime is rather inconvenient. In addition, one-photon ionization does not take advantage of bound energy levels of Yb in order to make this process isotope selective. Therefore, it is useful to first excite Yb to a bound excited state and subsequently ionize the excited atom.

Figure 1 depicts relevant low-lying energy levels in YbI. Starting from the $^1S_0$ ground state, several energy levels may serve as a first excitation level from which the actual ionization process occurs. The inter-combination line near 555.6 nm has been extensively studied [30, 31] as a starting point for a photoionization process. Unfortunately, this wavelength is presently not accessible using an inexpensive diode laser. Therefore, we concentrate on the optical
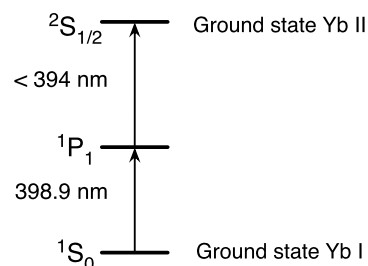
dipole transition from the ground state to the $^1P_1$ level near 398.9 nm. The $^1P_1$ state has a lifetime of 5.464 ns [19] and the transition $^1S_0$–$^1P_1$ is saturated by a light intensity of 60 mW/cm^2 [32]. Possible decay channels of the $^1P_1$ state are not indicated in Fig. 1, as the ratio between the rate for radiative decay into the ground state and the sum of the rates for decay into all other states is larger than 10^7 [33].

As indicated in Fig. 2, a second light field with wavelength below 394 nm is required to reach the continuum. This process has been proposed by Sankari and Suryanarayana [34], the principle of which has been demonstrated by us in earlier work [1]. Fortunately, this second light field is easily supplied by the cooling laser for the YbII ion near 369 nm, which is already present at experiments working with trapped YbII. This makes this scheme very practical indeed, as only one other diode laser needs to be set up. This process is termed two-color ionization and its experimental investigation is described in detail in Sect. 5.

This contrasts with the scheme presented in Sect. 6 that we label one-color ionization. As is shown experimentally, a second light field near 369 nm is not necessary to ionize YbI atoms in an ion trap; instead, employing only the laser near 398.9 nm is sufficient.

In the remainder of this section we will be concerned with the spectroscopy and isotope-selective excitation of the $^1S_0$–$^1P_1$ transition in YbI. The authors of Ref. [35] carried out careful spectroscopy of neutral ytterbium and provided absolute transition frequencies for the transitions of interest here.

Laser induced resonance fluorescence spectra of YbI are recorded using a thermal atomic beam emitted from three different ovens heated resistively. The ovens are molybdenum tubes with an inner diameter of 0.78 mm and a wall thickness of 0.2 mm, spot welded to a tantalum wire. The ground connection is cut from a tantalum foil (thickness 0.2 mm) with a size of approximately 2×4 mm^2, spot welded close to the opening of the oven tube. Two ovens contain samples of YbI that are isotopically enriched with ^{171}Yb and ^{172}Yb, respectively, while the third oven contains a sample with the natural abundance of isotopes of ytterbium. Two different experimental setups are used for the experiments reported in this article: the isotopically enriched ovens are mounted in a vacuum chamber maintained

at a pressure below 10^{-10} mbar (when the oven is turned off) that also houses a miniature Paul trap (compare Sect. 5.1). The third oven is contained in a vacuum chamber at a typical pressure of 5×10^{-9} mbar together with a linear Paul trap [1].

For excitation of the $^1S_0-^1P_1$ transition, a tuneable external cavity diode laser is used with an emission bandwidth of about $2\pi \times 500$ kHz. The wavelength of the laser radiation is measured using a wave meter to a precision of 0.05 pm using a temperature-stabilized HeNe laser as a reference corresponding to an uncertainty of ≈ 95 MHz in absolute frequency. The laser beam crosses the atomic beam at an angle close to $45°$ or $90°$.

Resonance fluorescence of YbI close to 399 nm is collected, imaged, and detected using the setups that are in use for photon counting the resonance fluorescence close to 369 nm originating from the $P_{1/2}-S_{1/2}$ transition in YbII. With the setup containing the isotopically enriched YbI ovens, light is collected using an objective with a numerical aperture of approximately 0.4 and then imaged onto a photomultiplier tube (Burle C31034A2) operated in photon-counting mode. The overall detection efficiency is about 1%. The setup with the oven containing ytterbium with natural abundance of isotopes uses optical elements for light collection with a numerical aperture of approximately 0.5 and a photomultiplier (Hamamatsu R5600P) with an overall calculated efficiency of 1.3% for the detection of light emitted by YbI and YbII.

2.1 Isotope-selective excitation of YbI

Figure 3 shows laser induced resonance fluorescence spectra of the $^1S_0-^1P_1$ transition in YbI. These were measured employing isotopically enriched samples of ^{171}Yb or ^{172}Yb. The abscissa indicates the frequency relative to the center of the resonance corresponding to ^{174}YbI that was found at a vacuum wavelength near 398.91 nm.

The excitation line profile in Fig. 3a is Doppler broadened and shifted while in Fig. 3b and c Doppler broadening is strongly reduced, with the measured line widths of $\Gamma_{172} = 2\pi \times 71(1)$ MHz and $\Gamma_{171} = 2\pi \times 89(1)$ MHz a factor of approximately 3 higher than the natural line width of $2\pi \times 28$ MHz due to saturation broadening and the Doppler broadening due to the divergence of the atomic beam. The hyperfine splitting of the $^1P_1$ level of the ^{171}Yb isotope is clearly resolved. Small peaks to the left and right of the respective main resonances in Fig. 3b and c are due to impurities from other isotopes.

After having obtained sufficient spectral resolution with the isotopically pure ^{171}Yb and ^{172}Yb ovens, a new oven with a natural abundance isotope distribution was built, and Fig. 4 shows the atomic resonance fluorescence spectrum measured with this oven. The spectrum was fitted to a sum
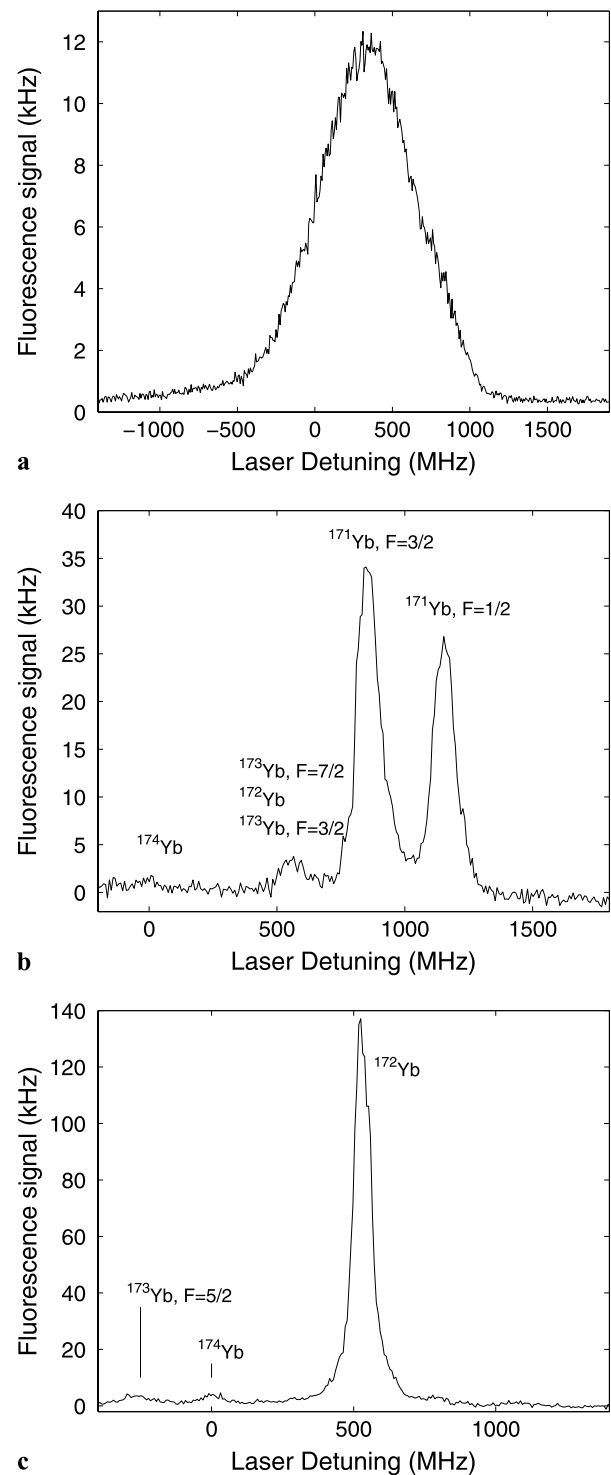
Fig. 3 Laser induced resonance fluorescence spectra of the $^1S_0-^1P_1$ transition in YbI. An isotopically enriched sample of ^{171}YbI (**a**, **b**) or ^{172}YbI (**c**) was used. The detuning of the laser frequency is given relative to the resonance of ^{174}Yb. (**a**) ^{171}YbI: the angle between the laser beam and the atomic beam is about 45 degrees. The resonance is shifted and broadened by the Doppler effect. (**b**) ^{171}YbI: the laser beam crosses the atomic beam at right angles allowing for resolution of the hyperfine structure. The rest abundance of ^{172}YbI can be seen as a small resonance peak to the left of the two prominent hyperfine resonances of ^{171}YbI. (**c**) ^{172}YbI: Doppler-reduced spectrum
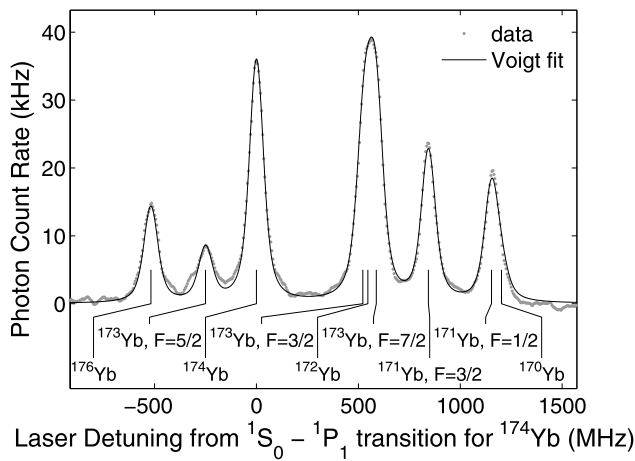
Fig. 4 Laser induced resonance fluorescence spectra of the $^1S_0$–$^1P_1$ transition in YbI with reduced Doppler broadening from an oven with natural abundance isotope distribution. All hyperfine information displayed at the resonances concerns the upper levels of the transitions since the ground state exhibits no hyperfine splitting. Nonlinear regression was performed by assuming fixed spacing given by [35] and fitting a common horizontal and vertical displacement, a natural line width, a residual Doppler width, and individual peak heights

of six Voigt profiles to obtain the isotope shift of the resonance frequencies and agreement within mutual error bars was found with [35]. In this spectrum, the different isotopes are resolved, allowing for selective ionization and hence trapping of different isotopes of ytterbium.

The resonance $^1S_0$–$^1P_1$, $F = 3/2$ corresponding to the isotope ^{173}YbI is separated from the $^1S_0$–$^1P_1$ resonance in ^{172}YbI by only 17 MHz [35]. Thus, it is difficult to spectrally resolve these two isotopes. However, if loading an ion trap with ^{172}YbII is desired, then this is not an obstacle, since the odd isotope's hyperfine structure prevents this ion from being efficiently laser cooled: if no microwave radiation is present that avoids optical pumping into a 'dark' hyperfine level (with respect to laser light near 369 nm driving the $S_{1/2}$–$P_{1/2}$ transition in YbII) of the electronic ground state, then it is unlikely that ^{173}Yb$^+$ at a thermal velocity is sufficiently laser cooled to be trapped. Furthermore, these ions would be visible as dark gaps in linear ion crystals. This has not been observed during the loading of ion crystals reported in Sect. 5.3.

Deterministic loading of only one isotope is, strictly speaking, never possible by spectral means—the Lorentzian wings of the absorption profile always leave a non-vanishing probability for excitation at all detunings, and only a certain degree of rejection of other isotopes can be achieved. It should be pointed out, however, that this level of discrimination is unfavorable for certain isotope combinations.

3 One-dimensional heat model of the oven

We have manufactured a variety of ovens with different geometries which all have in common that ytterbium inside a metal tube with one open end is evaporated by ohmic heating.

The latest ovens were designed to meet the special demand of a microstructured segmented linear ion trap. To avoid coverage of the trap chip with neutral ytterbium, the atomic beam should be restricted to a region narrower than the electrode separation. Initial experiments with squeezed oven nozzles gave good collimation results, confirmed by analyzing transverse Doppler-broadening profiles. But, within 30 h of operation, the Doppler width broadened gradually, most likely due to clogging or redeposition in the nozzle. Satisfying long-term behavior could be achieved by a laser-cut slit aperture a few millimeters apart from the oven nozzle.

Our recent ovens are made of a steel tube and wire, which is thinned at one point to give a high local ohmic loss. A steel tube, partially filled with a small amount of ytterbium, is mounted close to this point and a collimated ytterbium beam emerges from the open tube end. The feed wires are made of molybdenum.

A simple heat model for a small piece of wire states that the net flux of power per length element vanishes for a steady state temperature distribution:

$$dP_{ohm} - dP_{rad} - dP_{cond} = 0 \qquad (1)$$

with the infinitesimal power contributions dP due to ohmic heating, radiation, and conduction. These powers for a small length interval dx of a cylindrical wire are given as

$$dP_{ohm} = I^2 dR = \frac{I^2 \rho(x)}{\pi r^2} dx, \qquad (2)$$

$$dP_{rad} = dA\sigma\epsilon T^4 = 2\pi r\sigma\epsilon(T^4 - T_0^4)dx, \qquad (3)$$

$$dP_{cond} = dP_{cond}(x - dx/2) - dP_{cond}(x - dx/2)$$
$$= \kappa\pi r^2(T'(x + dx/2) - T'(x - dx/2))$$
$$= \kappa\pi r^2 T''(x)dx. \qquad (4)$$

In (2)–(4), the heating current is denoted as I, $\rho(x)$ is the electrical resistivity, r is the radius of the wire, σ is the Stefan–Boltzmann constant, ϵ is the emissivity of the wire material, T_0 is the ambient temperature, and the thermal conductivity is termed as κ. Inserting (2)–(4) into (1), one finds that the second derivative of the temperature has its origin in ohmic heating and radiative losses:

$$-\kappa\pi r^2 T''(x) + \frac{I^2\rho(x)}{\pi r^2} - 2\pi r\sigma\epsilon(T^4 - T_0^4) = 0. \qquad (5)$$
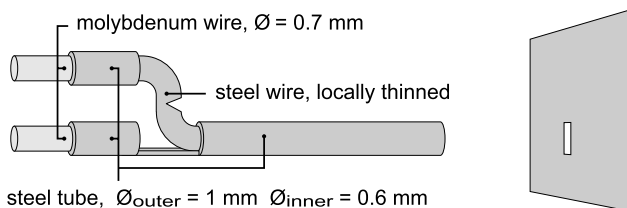
Fig. 5 Sketch of the oven

When the oven is modeled as a one-dimensional system made of the feed-through wire with a small incision as the heating element, the electrical resistivity along the wire is given by

$$\rho(x) = \rho_0 + R\pi r^2 \delta(x), \tag{6}$$

where ρ_0 is the resistivity of the wire and R is the resistance of the incision at $x = 0$ (treated as point like). We integrate (5) numerically, which allows us to account for the temperature dependence of electrical and heat conductivities using the Wiedemann–Franz law [36]. We take into account two boundary conditions: (i) the temperature at the holders at $x = \pm\ell$ equals the ambient temperature T_0 and (ii) the temperature distribution has a kink at the heating element at $x = 0$ and the derivative changes by $I^2 R/\kappa\pi r^2$.

Figure 6 shows a numerical solution for the temperature distribution using a current of 1.5 A and parameters that describe our oven adequately. These parameters are obtained either from the literature (as for κ and ρ) or from our own measurements (as for R). The parameters used for calculating and plotting the temperature distribution are: $r = 0.35$ mm, $\ell = 10$ cm, $R = 0.06$ Ω, $\rho = \rho_0 \times [1 + \alpha_{el}(T - T_0)] = 5.57 \times 10^{-8}[1 + 4.82 \times 10^{-3}(T - 298$ K$)/$K$]$ mΩ [37], $\kappa(T_0) = 138$ W/mK [38].

The distribution is found to be dominantly triangular, with negligible ohmic losses in the wire and small positive curvature for higher-temperature regions due to radiative losses. The model gives reasonable agreement with measurements of the oven tip temperature considering that we did not take into account the geometric details of our oven.

The oven tip temperature was measured close to the incision shown in Fig. 5 using a j-type thermocouple as a function of heating current (see Fig. 7) and a hyperbolic dependence is found. This functional dependence is unexpected at first sight: one would expect a quadratic behavior for small currents, as the heating power depends quadratically on the current, and radiative losses are negligible. In fact, such a dependence is found for small currents. For high currents one would expect a square-root dependence of the tip temperature, arguing that dominating radiative losses which scale as T^4 are balanced by a heating power behaving as I^2, but such a regime is not observed for the currents that we applied. An extended linear regime can be explained, however, taking
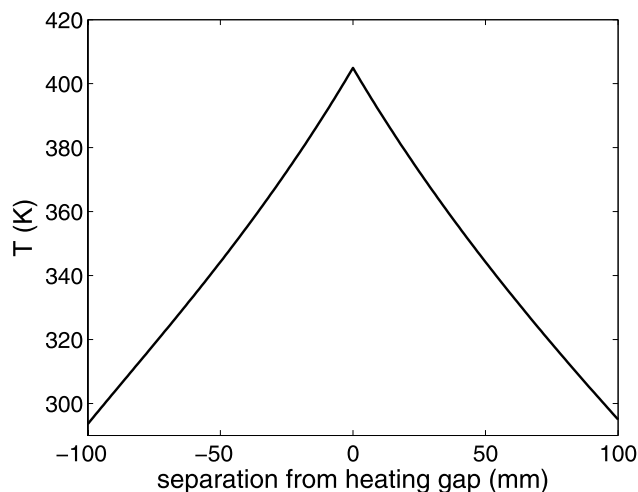

Fig. 6 Temperature distribution along a wire with an incision at $x = 0$ and held at room temperature at $x = \pm 10$ cm
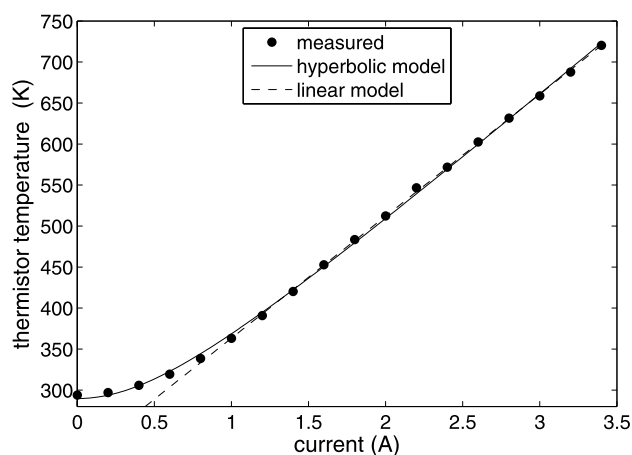

Fig. 7 Temperature of the oven tip as a function of heating current

into account the temperature distribution along the wire as above. The hyperbolic dependence is reproduced by a simple analytical model assuming a triangular temperature distribution in accordance with the results shown in Fig. 6:

$$T(x) = T_{max} - \frac{T_{max} - T_0}{\ell}|x|, \quad |x| \leq \ell \tag{7}$$

with the ambient temperature T_0. The heat loss through the wire ends at $|x| = \ell$ equals $2\kappa\pi r^2 T'$ and power balance requires

$$I^2 R = 2\kappa\pi r^2 T' + \int_{-\ell}^{\ell} 2\pi r\sigma\epsilon \left(T(x)^4 - T_0^4\right) dx \tag{8}$$

$$= 2\kappa\pi r^2 T' + \frac{4\pi r\sigma\epsilon\ell}{5(T_{max} - T_0)}\left(T_{max}^5 - T_0^5\right). \tag{9}$$

After division of the radiative term by a polynomial and considering terms up to second order in T_{max}, the peak temper-

ature is obtained as

$$T_{\max} \approx \left(\frac{T_0}{2} - \alpha \right) + \sqrt{\left(\frac{T_0}{2} + \alpha \right)^2 + \beta I^2} \tag{10}$$

with the constants α and β given by

$$\alpha = \frac{\kappa}{8\ell^2 T_0^2 \epsilon \sigma}, \qquad \beta = \frac{R}{\pi r \lambda} \alpha, \tag{11}$$

which gives the observed hyperbolic dependence. We have measured the temperature of the oven tip with a vacuum-compatible thermistor and find good agreement with a hyperbolic model. For a current above 1 A (that leads to a useful atom flux, as will be reported below), a linear relation between current and temperature is found. It should be noted that the measured quantitative asymptotic behavior is not predicted by the coefficients extracted from (11), most likely due to geometric details and material properties that are neglected or simplified in our model. However, the important general insight remains that heat conductivity and radiative losses yield a polynomial expression in $T_{\max} - T_0$ in (9) which results in a hyperbolic dependence of the maximum temperature as a function of heating current.

4 Neutral atom densities and atomic flux

The temperature of ytterbium in a closed oven would result in a vapor pressure, which, for a temperature-independent latent heat, is predicted by the Clausius–Clapeyron equation to take the simple form

$$p_{\mathrm{vp}}(T) = p_0 \mathrm{e}^{-T_1/T}. \tag{12}$$

The coefficients of a slightly extended model were optimized to match experimental data in the range 10^{-10} Pa to 10^2 Pa within 5% [39]. Assuming the ytterbium vapor to behave as an ideal gas, the particle density can be calculated from the vapor pressure:

$$n = \frac{p_{\mathrm{vp}}(T)}{k_{\mathrm{B}} T} = \frac{p_0 \mathrm{e}^{-T_1/T}}{k_{\mathrm{B}} T}. \tag{13}$$

Furthermore, for a Maxwellian distribution of atom velocities, one can calculate the flux of atoms through a circular aperture with radius r:

$$\dot{n} = \sqrt{\frac{8\pi r^4}{m k_{\mathrm{B}} T}} p_0 \mathrm{e}^{-T_1/T} = \frac{\pi r^2}{k_{\mathrm{B}} T} \langle v \rangle p_0 \mathrm{e}^{-T_1/T} \tag{14}$$

with the mean velocity of the atoms in the beam

$$\langle v \rangle = \sqrt{\frac{8 k_{\mathrm{B}} T}{\pi m}}. \tag{15}$$

When calculating densities and fluxes from currents using (10) and (12)–(14), one has to bear in mind that the effective temperature might in general be lower than the one obtained for the heating element, since the atoms can thermalize with the whole, and generally cooler, oven tube.

Atom densities and fluxes were characterized for the oven which was optimized for use with a microstructured segmented linear Paul trap. The neutral atom fluorescence is imaged onto a small aperture, which in turn is imaged onto a photomultiplier. Magnification and aperture are chosen such that the intensity and atom density can be assumed approximately constant over the detected area. We take into account saturation by determining experimentally the intensity profile of the laser and the total power. For all measurements, we assume a steady state temperature distribution which is ensured by a 10-min warm-up.

The measured current dependence (Figs. 8 and 9) of the density and flux is fitted by a simple model: the atomic vapor is in thermal equilibrium with the oven. The oven has an effective temperature, which is assumed to exhibit a linear dependence on current as found with thermistor measurements for higher currents (compare Fig. 7). The dependence of the effective oven temperature is not necessarily identical with the dependence of the oven tip temperature: we allowed for a temperature offset and a different slope; in general, the effective temperature is expected to be lower than the one measured by the thermistor. The temperature is used to calculate the vapor pressure and flux. Both quantities are multiplied by a factor, taking into account the finite atomic beam divergence, non-equilibrium effects, imperfect characterization of our detection efficiency and saturation.

The model describes the measurements quite well. It states that the effective temperature of the oven (and thus the atoms' temperature) shows the same slope with respect to the current, but is substantially lower than the temperature of the oven tip (by approximately 50 K).

5 Two-color ionization of YbI

In this section we report on resonance-enhanced isotope-selective ionization of YbI with subsequent loading of the ions into a Paul trap (ring trap or linear trap). The possibility to selectively excite a certain isotope out of a mixture of natural abundance material is an advantage of photoionization. This selectivity is achieved by the first excitation step from the ground state of YbI into the $^1P_1$ state as reported in the previous section. The second excitation step from the $^1P_1$ state of YbI into the ionization continuum is achieved by means of laser light near 369 nm (Fig. 2). The dependence of trap loading efficiency on laser intensities, laser frequencies, and relative flux of neutral atoms is studied.
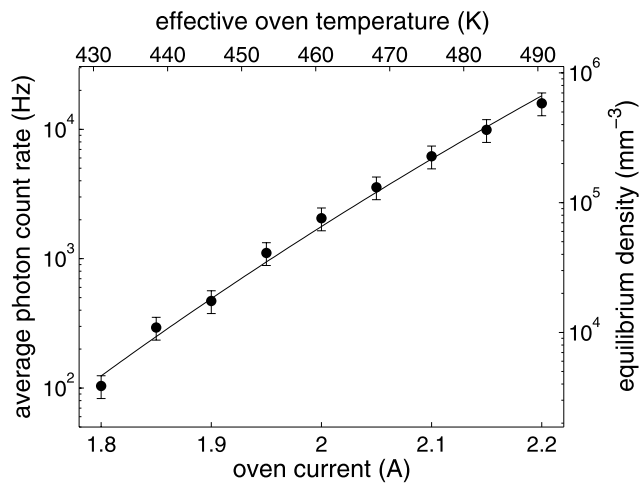
Fig. 8 The atom density from a collimated ytterbium beam with natural isotope abundance as a function of oven heating current. The beam is collimated by an aperture separated 3 mm from the oven nozzle. The density was measured approximately 5 mm away from the collimating aperture
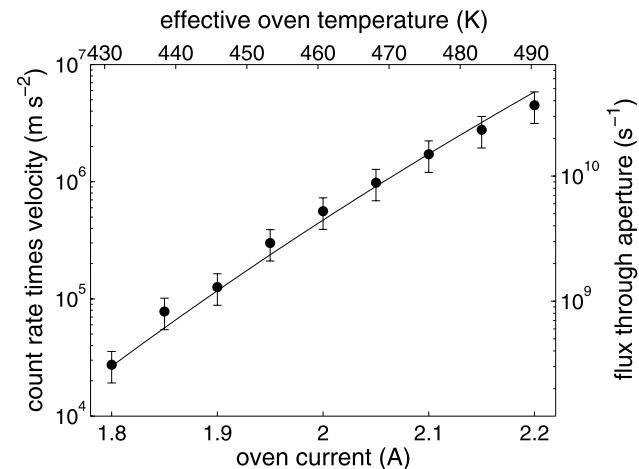

Fig. 9 The atomic flux density from a collimated ytterbium beam with natural isotope abundance as a function of oven heating current. The density data presented in Fig. 8 was combined with measurements of the line shift due to the mean beam velocity as shown in Fig. 3a

5.1 Experimental procedure

A part of the experimental setup was described already in the preceding section that deals with resonant excitation of YbI. Now, taking advantage of this isotope-selective excitation of the $^1P_1$ state, we are concerned with photoionization of YbI and trapping of YbII. Ions are trapped in either a miniature ring Paul trap or a linear Paul trap. The ring trap electrodes are made from molybdenum wire with a diameter of 0.3 mm. The ring electrode has an inner diameter of 2.0 mm and the end cap electrodes are 1.4-mm apart. An rf field at 9.5 MHz with peak amplitude of about 700 V is applied between ring and end cap electrodes. The linear trap is

made of four molybdenum rod electrodes 0.5 mm in diameter, held by two Macor plates spaced 6-mm apart. The radial distance from the axis to the surface of the rods is 0.75 mm. Two molybdenum end caps with a diameter of 0.4 mm serve for axial confinement, and are spaced 4.1-mm apart. An rf field with frequency between 10 and 20 MHz and amplitude of up to 2 kV is applied to the rod electrodes for radial confinement, and a low voltage of several volts only is applied for axial confinement. Typical secular frequencies are 30–60 kHz in the axial direction and 600–800 kHz radially.

Light near 369 nm driving the $S_{1/2}$–$P_{1/2}$ transition in YbII is supplied by a frequency-doubled commercial Ti:Sa laser (Coherent MBR110) which provides about 400 W m focused to a spot size of approximately 100 μm ($1/e^2$ diameter of the intensity). A diode laser delivers light near 935 nm and drives the $D_{3/2}$–$[3/2]_{1/2}$ transition in YbII to avoid optical pumping into the metastable $D_{3/2}$ state [40].

An electric current resistively heats the oven and, after some time, a stationary temperature is obtained. Therefore, each oven was heated for at least 10 min prior to the actual experiment, unless stated otherwise. The oven temperature determines the vapor pressure and atom density inside the oven and the atomic flux density in the particle beam that emerges from the open end of the oven.

In order to determine quantitatively the atomic number density in the trapping region of the ion trap, one would need knowledge of (i) the spatial profiles of the atomic beam and the laser beam in the region where they cross, (ii) the overall detection efficiency of the system measuring the resonance fluorescence in this crossing region as a function of the position of the fluorescing atoms (the depth of focus for the optics collecting the fluorescence is rather small due to a large numerical aperture), and (iii) the transition line strength of the $^1S_0$–$^1P_1$ transition. Thus, deducing the number density from the observed resonance fluorescence spectra is in principle feasible, albeit with a large systematic error. If the number density were known, the investigation of ion loading rates as a function of oven current reported below could be presented as a function of neutral atom density instead. The ion loading rates depend, in addition, on (i) the ionization cross section for the different ionization schemes reported (one-color, two-color, electron impact), (ii) the quasi-static electric field experienced by the atoms in the trap region that varies spatially and in time in a different manner for each trap, and (iii) the rate at which different YbII ions are laser cooled, which in turn is a function of the spatial profiles and overlap of the laser beams near 369 nm and 935 nm used for laser cooling YbII and their frequency, intensity, and polarization (in addition, for odd isotopes also of the parameters characterizing the microwave radiation necessary to avoid optical pumping). We do not attempt here to give a full quantitative description that might be plagued by a large uncertainty while not altering the conclusions drawn from the measurements reported below.
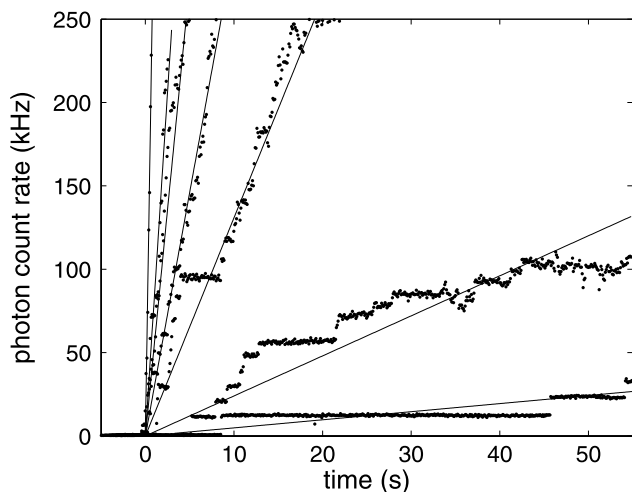
Fig. 10 Two-color photoionization of ^{172}YbI as a function of time for different electric currents heating the atom oven. The fluorescence signal is proportional to the number of trapped YbII ions for a low number of ions, i.e. short loading times (here, a single ion produces a photon count rate of $\approx$15 kHz). In this region the signals are fitted by a linear function to extract loading rates as a function of oven current. Steps in the photon count rate for small heating currents indicate an increase by one of the number of trapped ions. The oven currents were (in order of ascending signal slope): 1.8 A, 1.9 A, 2.0 A, 2.18 A, 2.3 A, 2.47 A, 2.57 A

Fig. 11 Comparison of efficiency for electron impact and two-color ionization of ^{172}YbI (oven current set to 2.5 A) [1]. The upper trace (*dots*) shows the rise in fluorescence when two-color photoionization is used and a fit (*solid line*) to the linear slope of the signal as in Fig. 10 (note that the linear slope is not displayed as a straight line due to the logarithmic depiction). The step in the lower time trace (electron impact ionization) signifies the trapping of a single ion

The wavelength of the laser near 398.9 nm was set to a value corresponding to the $^1S_0$–$^1P_1$ resonance of the desired isotope to be loaded into the trap, and the peak laser intensity (Gaussian beam profile) in the ionization region was 3 W/cm^2, if not explicitly stated otherwise.

When both the lasers near 369 nm and near 398.9 nm are directed into the trap region, the atomic resonance fluorescence signal is added on top of the ionic fluorescence. Experimentally, the signals due to YbI and YbII are discernible by blocking temporarily the repump laser at 935 nm, which leads to optical pumping into the metastable D$_{3/2}$ state of YbII and thus the ionic fluorescence is interrupted. Typically, the fluorescence signal collected from neutral atoms amounts to—depending on oven current—several tens of kHz.

5.2 Two-color ionization

Figure 10 shows combined atomic (YbI) and ionic (YbII) fluorescence signals in dependence on the ionization time and the oven current for two-color ionization. The procedure to record the time series in Fig. 10 is as follows: the ion trap is emptied by turning off the rf trapping field and all lasers except the excitation laser at 398.9 nm are turned on. After 3 s the excitation laser is unblocked, leading to fast loading of the trap and accordingly to an increase in the ionic fluorescence signal. With a fluorescence rate of 15 kHz for a single ion here, on the order of 100 ions are trapped in the
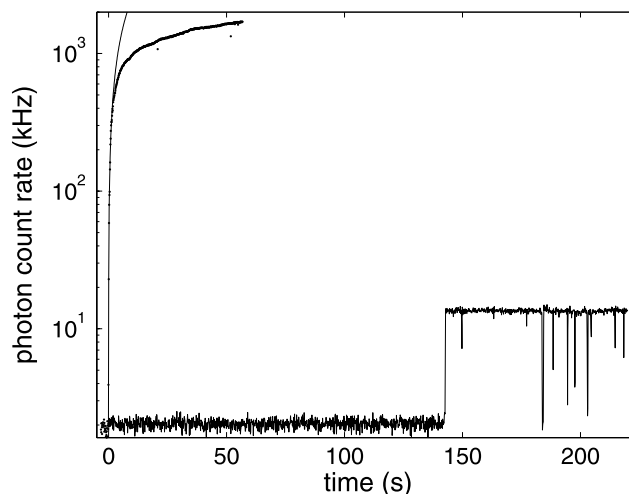
first 15 s for the highest oven current at 2.57 A, indicating the high efficiency of this process. This oven current represents the usual value used with electron impact ionization.

The resonance fluorescence signal begins to saturate, after a time depending on oven current, generally for ion numbers greater than about 20, owing both to the limited trapping capacity and the reduced efficiency of the optics for imaging a large ion 'cloud' (the optical setup used here is optimized for imaging a single ion located in the center of the trap). A limited capacity for trapping can be attributed to the laser beam waist being too small to illuminate large clouds. In addition, large hot clouds exhibit a large number of micromotion sidebands, such that the scattering of resonance fluorescence induced by a laser with narrow emission bandwidth is reduced dramatically.

The oven current is varied between 1.80 A and 2.57 A. For those currents, we obtained feasible loading rates and low vacuum contamination. As expected, the rate of loading ions increases with the atom flux density. Depending on the probability for ionizing a neutral atom passing by, two dependences are conceivable: for almost unit probability of ionization, the loading rate will be proportional to the atom flux, whereas for low probability of ionization, the loading rate can be expected to behave proportionally to the atom density. A comparison of loading rates on the order of a few per second and much higher measured fluxes shows that the latter is the appropriate model, and Fig. 12 shows the measured loading rate together with a fit that assumes proportionality to the atom density.

In Fig. 11 the loading rate using two-color photoionization is compared with electron impact ionization. The time
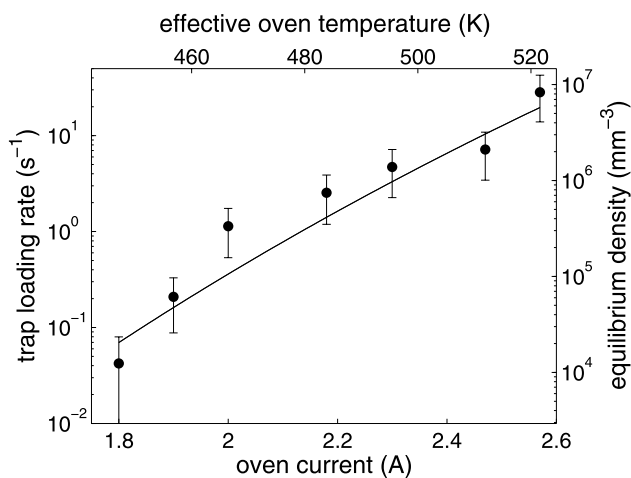
Fig. 12 Loading rate extracted from the slope of fluorescence increase in the linear regime as a function of oven current (compare Fig. 10). A thermodynamic vapor density is fitted to the data assuming a linear dependence between current and effective temperature as observed from probe measurements (see Sect. 4). The fitted dependency is comparable to the one measured in Sect. 4, even though the oven was constructed with a slightly different design

Fig. 13 Dependence of the ionic resonance fluorescence signal—and hence the loading rate—on detuning of both lasers for two-color photoionization during the loading time. The fluorescence signal shows a strong dependence on the detuning of the 399-nm laser (*filled dots*), since this excitation is a resonant process. The *solid line* indicates a fit using a Voigt profile. The non-resonant excitation with the 369-nm laser above ionization threshold shows no dependence on variation of wavelength (*open circles*) and can be fitted by a constant (*dashed line*). The ionization time was 30 s at 2.59-A oven current

series indicating the fluorescence signal when using electron impact ionization shows a sharp increase at about 142 s that signifies the trapping of a *single* ^{172}Yb ion. In contrast, the ionic signal rises quickly when using photoionization, indicating trapping of more than 100 ions during the first seconds after turning on the excitation laser. The two-color-ionization process results in an estimated increase in trap loading rate of about 3000 in comparison with electron impact ionization. For this measurement, the oven current was set to 2.5 A.

In the two paragraphs to follow we examine the influence of the frequency of both the laser light field near 369 nm and the one near 399 nm on the efficiency of the ionization process. The ionization model depicted in Fig. 2 is corroborated by these measurements.

Figure 13 shows the resonance fluorescence signal of trapped ^{172}Yb ions under variation of the frequency of the cooling laser close to 369 nm over a range of 800 MHz during the loading phase. The scan was taken with the oven current set to 2.59 A and 30-s ionization time. During the observation stage of the trapped ions, the laser at 369 nm was set close to resonance. The observed fluorescence signal is consistent with a structureless flat dependence of the ionization rate on the detuning of the cooling laser near 369 nm in the frequency range depicted here. This is in accord with the ionization model that the atom is excited from the $^1P_1$ state into the ionization continuum (Fig. 2). The energy of the photon at 369 nm is larger than the energy needed to reach the continuum (equivalent to a wavelength of 394 nm); thus, no dependence on small frequency variations is expected.
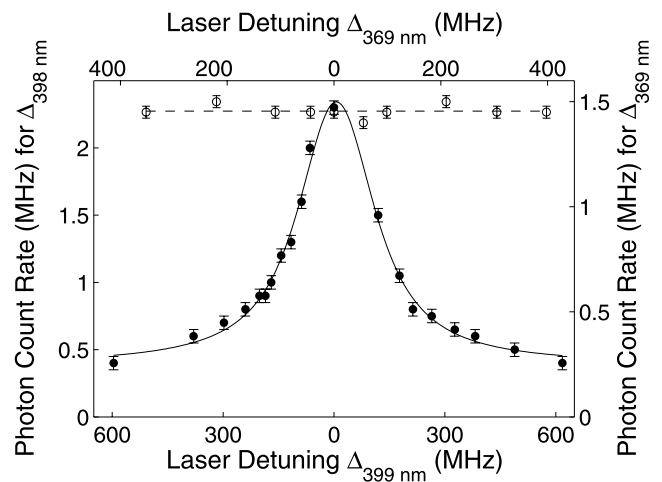
On the other hand, based on the excitation spectra of neutral YbI the detuning of the excitation laser at 398.9 nm is expected to have a distinct influence on the ionization efficiency for a given isotope. The second data set in Fig. 13 confirms this assumption. There, the excitation laser is scanned over a range of 1.2 GHz and the resulting *ionic* fluorescence is recorded. This graph may also be compared to Fig. 3a, since both data sets were taken using the ^{171}Yb isotope and an angle of 45 degrees between the atomic and laser beams, respectively (thus, the line profile is dominated by Doppler broadening). The oven current was set to 2.82 A and the time during which the excitation laser was turned on was 60 s.

5.3 Nearly deterministic loading of an ion trap

The last paragraph of this section deals with an experimentally important feature of photoionization of YbI for ion trap experiments: it is desirable to (nearly) deterministically load a desired number of ions into the trap. In addition, the flux of neutral atoms possibly contaminating trap structures should be significantly reduced. So far, the oven current was set to a certain value and kept there to allow for comparison of different loading rates. Now, when trying to quickly load ions, all laser frequencies and intensities are set first before the oven current is turned on. The wavelength of the excitation laser near 399 nm is set with an accuracy better than 80 MHz using a wave meter, which is sufficient to find the atomic resonance without having to rely on the atomic beam. Thus, already the first atoms emitted from the oven have a chance
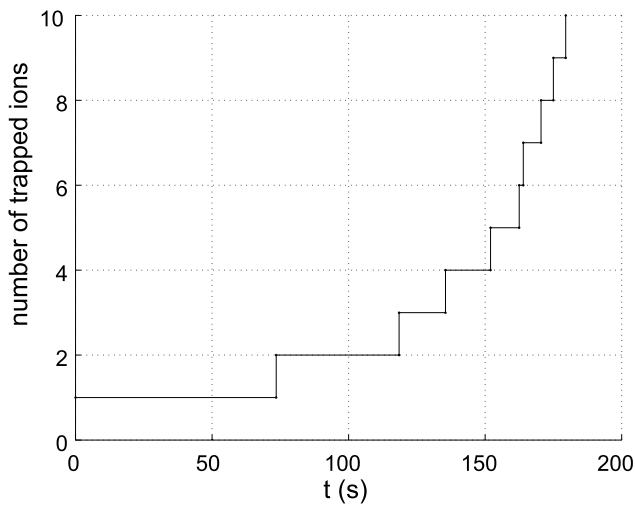
Fig. 14 Deterministic loading of a desired number of ions by two-color photoionization [1]. The loading rate increases with time, since the oven emitting YbI atoms heats up during the measurement

of being ionized by efficient two-color ionization and are immediately laser cooled by the same laser light that ionizes them. It turns out that the loading rate using this procedure is such that any desired (low) number of ions is easily selected simply by blocking the ionization laser at the right time.

Figure 14 shows the number of trapped ions plotted against time. This experiment was performed with a linear Paul trap and the ionic fluorescence was detected by an image-intensified CCD camera. The number of visible ions and their locations allow us to extract the ion number redundantly, if no dark ions are trapped. The time before the first ion is detected varies between 60 and 180 s after the oven current is turned on, depending on laser parameters. Then, while the oven is being heated the loading rate increases. This graph shows that nearly deterministic loading of a desired number of ions is possible using this procedure. To achieve that, the loading rate is set to be low (to reduce to probability of having additional hot ions in the trap, which appear in the cold ion string shortly after) and a feedback mechanism shuts off the laser near 399 nm, once the desired ion number has been achieved. A spatially resolved detection can also be used to automatically discard ion strings with impurity atoms from unwanted isotopes.

6 Single-color ionization of YbI

The energy carried by two photons at 398.9 nm is not sufficient to bridge the energy gap between the ground state of YbI and the ionization continuum. Therefore, it came initially as a surprise that YbII ions could be produced using this laser light alone.

For the experiments presented in this section all lasers are blocked first for a prescribed time while the laser at

399 nm is on. Then the laser exciting the atomic resonance is blocked while the lasers near 935 nm and 369 nm are turned on for cooling and detecting the ion.

Comparing the two methods shows that for the experimental parameters used here, the two-color ionization is almost two orders of magnitude more effective than the one-color ionization. In the latter case, though, the ions are cooled only after the ionization process is finished when the cooling laser near 369 nm is unblocked. For the two-color scheme, on the other hand, the ions are cooled as soon as they are ionized.

As an explanation of why ions are produced by 399-nm light alone, three-photon ionization would be conceivable, with the first photon exciting the atomic $^1S_0$–$^1P_1$ resonance as before, and two more photons ionizing the atom. This 'second' two-photon process could again be resonance enhanced, if the 399-nm light excites a Rydberg state in YbI. If the absorption of the last two photons is *not* resonance enhanced, then a rough estimate shows that at a light intensity of a few watts per cm^2 this three-photon-ionization rate (proceeding resonantly with the first photon through the $^1P_1$ state and then with two more photons *non*-resonantly into the continuum) should be about 12 orders of magnitude lower than the two-photon rate (i.e. proceeding resonantly with the first photon through the $^1P_1$ state and then with *one* more photon into the continuum) [41]. Since such a low ionization rate is not consistent with our experimental observation, we conclude that a three-photon process that is not a second time resonance enhanced cannot be responsible for the observed production of YbII using light near 399 nm.

Is there a Rydberg state that could be resonantly excited starting from the $^1P_1$ state with the same light that excites the $^1S_0$–$^1P_1$ transition, and thus lead to a three-photon process that is resonantly enhanced a second time? From this Rydberg state, a third photon at the same wavelength would then ionize the atom. Starting from the $^1P_1$ level the dipole-selection rules allow transitions into either S- or D-Rydberg states. Checking the energy levels of the S- and D-Rydberg series shows that no level exists at 50136.444 cm^{-1}, the energy corresponding to two photons near 398.9 nm [42, 43]. The nearest unshifted singlet states are the $6s23s\,^1S_0$ at 50130.98 cm^{-1} and the $6s22d\,^1D_2$ at 50148.59 cm^{-1}, with an energy difference to the value above of 5.46 cm^{-1} and 12.15 cm^{-1}, respectively. We therefore exclude resonant excitation of an *unshifted* Rydberg state as a likely candidate for the observed photoionization by a one-color light field.

When considering possible ionization pathways we have neglected so far the influence of the rf trapping field on the ionization process. Given the trap dimension of the ring trap and the applied rf voltage, the peak electric field is estimated as 7×10^5 V/m. With the Stark shift taking on a value of about 10^{-6} Hz/(V/m)^2 for hydrogen with $n = 2$ and being proportional to n^7 (with principal quantum number n) [44],

it is expected that the Stark shift of the $^1P_1$ state is negligible here while Rydberg states with $n \approx 22$ are considerably shifted in energy. In fact, the trapping potential lowers the ionization threshold such that a second photon at 398.9 nm directly reaches the continuum.

In a simplified picture a hydrogen atom exposed to a constant external electric field in the direction x shows an asymmetric binding potential along this direction as

$$V = -\frac{e^2}{4\pi\epsilon_0}\frac{1}{x} - eEx \qquad (16)$$

with elementary charge e, electron nucleus separation x, and magnitude of the external electric field E. The potential maximum in the direction of the electric field is lowered with respect to the unperturbed atom, which corresponds to a lowering of the ionization threshold by

$$\Delta U = \sqrt{\frac{e^3 E}{\pi\epsilon_0}}. \qquad (17)$$

This is reminiscent of the Schottky effect [45], which describes the lowering of the work function of solid-state materials in the presence of an electric field.

The difference of the ionization energy $U = 50443$ cm^{-1} and the energy of two photons $2E_{398} = 50136.4$ cm^{-1} requires a lowering of the ionization energy by at least $\Delta U = 306.6$ cm^{-1}. Using (17), this corresponds to a required field strength exceeding $|E_{ph}| = 2.5 \times 10^5$ V/m.

On the other hand, the peak potential in a linear ion trap along the z direction is given by

$$\phi_{peak} = U_0 \frac{x^2 - y^2}{r_0^2} \qquad (18)$$

with the peak voltage U_0 and the electrode separation $2r_0$, yielding a peak electric field of

$$E_{peak} = -|\nabla\phi| = \frac{2U_0}{r_0^2}\sqrt{x^2 + y^2} = 2U_0\frac{r}{r_0^2}. \qquad (19)$$

Thus, the radius at which the required electric field strength for one-color photoionization is exceeded amounts to

$$r = \frac{|E_{ph}|r_0^2}{2U_0}, \qquad (20)$$

which gives for our trap ($U_0 = 1000$ V and $2r_0 = 1.5$ mm) a separation from the trap center of $r = 140$ μm. This gives 0.75 eV of initial quasi-potential energy which has to be laser cooled.

A full quantitative treatment of the electric field enhanced photoionization has to account, in particular, for the density and velocity distributions of the YbI atoms moving through the oscillatory trapping field, and the exact spatial dependence of the trapping field.
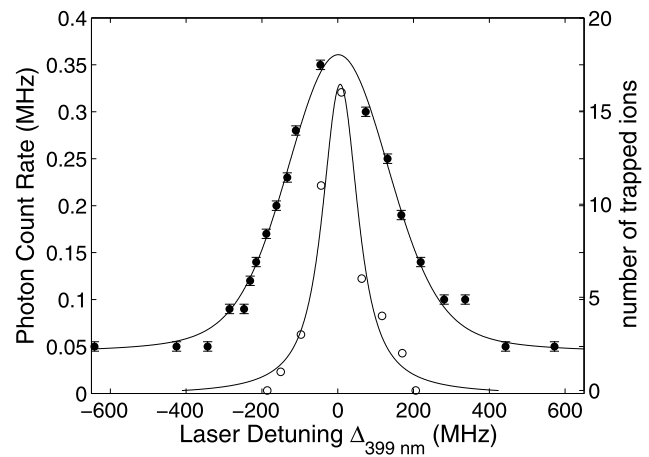

Fig. 15 Ionization efficiency of one-color photoionization of ^{172}Yb as a function of detuning of the 399-nm light from the $^1S_0$–$^1P_1$ resonance. The *filled circles* show the fluorescence signal as a function of laser detuning, similar to Fig. 13. The ionization time was 30 s at an oven current of 2.59 A and laser and atomic beams enclose an angle of 45 degrees. Fitting a Voigt profile yields a FWHM of 320 MHz. The *open circles* display the number of trapped ions after a loading time interval of 30 s at 2.79-A oven current. Here laser and atomic beams are perpendicular yielding low Doppler broadening. Fitting a Voigt profile yields a FWHM of 110 MHz, which is consistent with fluorescence profiles from neutral ^{172}Yb

The significantly lower trap loading rate when using 399-nm light alone for photoionization, as compared to the two-color process, is explained when considering (i) that only a fraction of the atoms interacting with 399-nm light have their ionization threshold sufficiently lowered to be ionized and (ii) the fact that during the short time interval between turning off the laser near 399 nm and turning on the lasers necessary for cooling YbII a fraction of the ions will have already left the trapping region.

Figure 15 shows the dependence of the loading process as a function of the detuning of the light near 399 nm from the $^1S_0$–$^1P_1$ resonance in ^{172}YbI. One data set (filled circles) was taken with an oven current of 2.59 A and an ionization time of 30 s. Due to an angle of 45 degrees between laser and atomic beams, the line width (FWHM 320 MHz) shows substantial Doppler broadening (when comparing this with Fig. 3a it should be noted that Fig. 3a shows a resonance fluorescence spectrum of ^{171}Yb, while the data in Fig. 15 shows the ionization of ^{172}Yb as a function of laser detuning). The second scan was taken with the laser beam perpendicular to the atom beam, an oven current of 2.79 A, and an ionization time of 30 s. The line width displayed here (FWHM 110 MHz) is consistent with the width of the atomic resonance line recorded as shown in Fig. 3c with ^{172}YbI. Thus, the ionization rate as a function of frequency of the laser light field near 399 nm is consistent with the absorption of the first photon ($^1S_0$–$^1P_1$ transition) being a resonant process and the second photon absorption ending in the ionization continuum.

7 Conclusion

We reported on two photoionization processes for neutral ytterbium that allow for loading of Yb^+ ions into a Paul trap. Both methods are implemented using just one additional diode laser near 399 nm. Laser diodes exist for this wavelength, and are close to the DVD standard at 405 nm. Since the saturation intensity of the $^1S_0$–$^1P_1$ transition in neutral Yb is rather small, a diode delivering on the order of 10 mW is sufficient for efficient ionization. Thus, a usual diode laser system in external cavity setup characterized by a small emission line width and easy to tune suffices to implement efficient photoionization of Yb.

The second step in the photoionization process (after excitation of the $^1S_0$–$^1P_1$ resonance) is achieved by absorption of a photon near 369 nm, the same light field used for cooling and detection of YbII ions. Therefore, it is ensured that the ionization process takes place in a region where the ion is immediately laser cooled and thus trapped and detected.

In addition, it is demonstrated that in the presence of the rf field used for trapping ions in a Paul trap, the light field near 399 nm alone suffices for a second excitation step into the ionization continuum shifted by the quasi-static electric field applied to the trap electrodes.

The isotope shift of the $^1S_0$–$^1P_1$ transition in neutral YbI is resolved in excitation spectra when reducing Doppler broadening by crossing the atomic and the laser beams at an angle near 90°. Thus, isotope-selective ionization is possible. The efficiency of two-color photoionization is found to be larger by a factor of 3000 in comparison with electron impact ionization for the experimental setup used in these experiments. We showed that (nearly) deterministic loading of a desired number of YbII ions into a linear Paul trap is feasible.

References

1. C. Balzer, A. Braun, T. Hannemann, C. Paape, M. Ettler, W. Neuhauser, C. Wunderlich, Phys. Rev. A **73**, 041407(R) (2006)
2. F. Strumia, in *Proc. 32nd Annu. Symp. Frequency Control* (Electronic Industries Association, Washington, 1987)
3. R. Blatt, H. Schnatz, G. Werth, Phys. Rev. Lett. **48**, 1601 (1982)
4. G. Werth, Metrologia **22**, 190 (1986)
5. R. Blatt, R. Casdorff, V. Enders, W. Neuhauser, P.E. Toschek, in *Proc. 4th Symp. Frequency Standards and Metrology* (Springer, Berlin, 1989), p. 306
6. H.A. Klein, A.S. Bell, G.P. Barwood, P. Gill, Appl. Phys. B **50**, 13 (1990)
7. P.T.H. Fisk, M.A. Lawn, C. Coles, Appl. Phys. B **57**, 287 (1993)
8. D.J. Seidel, L. Maleki, Phys. Rev. A **51**, R2699 (1995)
9. P. Gill, G.P. Barwood, H.A. Klein, G. Huang, S.A. Webster, P.J. Blythe, K. Hosaka, S.N. Lea, H.S. Margolis, Meas. Sci. Technol. **14**, 1174 (2003)
10. T. Schneider, E. Peik, C. Tamm, Phys. Rev. Lett. **94**, 23080 (2005)
11. R. Huesmann, C. Balzer, P. Courteille, W. Neuhauser, P.E. Toschek, Phys. Rev. Lett. **82**, 1611 (1999)
12. T. Hannemann, D. Reiss, C. Balzer, W. Neuhauser, P.E. Toschek, C. Wunderlich, Phys. Rev. A **65**, 050303 (2002)
13. C. Wunderlich, C. Balzer, Adv. At. Mol. Opt. Phys. **49**, 293 (2003)
14. D. Kielpinski, M. Cetina, J.A. Cox, F.X. Kärtner, Opt. Lett. **31**, 757 (2006)
15. R. Ozeri, W.M. Itano, R.B. Blakestad, J. Britton, J. Chiaverini, J.D. Jost, C. Langer, D. Leibfried, R. Reichle, S. Seidelin, J.H. Wesenberg, D.J. Wineland, Phys. Rev. A **75**, 042329 (2007)
16. P. Maunz, D.L. Moehring, S. Olmschenk, K.C. Younge, D.N. Matsukevich, C. Monroe, Nat. Phys. **3**, 538 (2007)
17. M. Cetina, A. Grier, J. Campbell, I. Chuang, V. Vuletic, Phys. Rev. A **76**4 (2007)
18. Y. Takasu, K. Honda, K. Komori, T. Kuwamoto, M. Kumakura, Y. Takahashi, T. Yabuzaki, Phys. Rev. Lett. **90**, 023003 (2003)
19. Y. Takasu, K. Komori, K. Honda, M. Kumakura, T. Yabuzaki, Y. Takahashi, Phys. Rev. Lett. **93**, 123202 (2004)
20. V. Natarajan, Eur. Phys. J. D **32**, 33 (2005)
21. W. Neuhauser, M. Hohenstatt, P. Toschek, H. Dehmelt, Phys. Rev. Lett. **41**, 233 (1978)
22. D.J. Wineland, R.E. Drullinger, F.L. Walls, Phys. Rev. Lett. **40**, 1639 (1978)
23. A. Mortensen, J.J.T. Lindballe, I.S. Jensen, P. Staanum, D. Voigt, M. Drewsen, Phys. Rev. A **69**, 042502 (2004)
24. N. Kjærgaard, L. Hornekær, A. Thommesen, Z. Videsen, M. Drewsen, Appl. Phys. B **71**, 207 (2000)
25. S. Gulde, D. Rotter, P. Barton, F. Schmidt-Kaler, R. Blatt, W. Hogervorst, Appl. Phys. B **73**, 861 (2001)
26. D.M. Lucas, A. Ramos, J.P. Home, M.J. McDonnell, S. Nakayama, J.-P. Stacey, S.C. Webster, D.N. Stacey, A.M. Steane, Phys. Rev. A **69**, 012711 (2004)
27. M. Brownnutt, V. Letchumanan, G. Wilpers, R.C. Thompson, P. Gill, A.G. Sinclair, Appl. Phys. B **87**, 411 (2007)
28. L. Deslauriers, M. Acton, B.B. Blinov, K.A. Brickman, P.C. Haljan, W.K. Hensinger, D. Hucul, S. Katnik, R.N. Kohn, P.J. Lee, M.J. Madsen, P. Maunz, S. Olmschenk, D.L. Moehring, D. Stick, J. Sterk, M. Yeo, K.C. Younge, C. Monroe, Phys. Rev. A **74**, 063421 (2006)
29. W. Meggers, J. Res. Natl. Bur. Stand. **83**, 396 (1978)
30. A. Tkachev, S. Yakovlenko, Quantum Electron. **26**, 839 (1996)
31. S.K. Borisov, M.A. Kuzmina, V.A. Mishin, Quantum Electron. **28**, 169 (1998)
32. R. Maruyama, Optical trapping of ytterbium atoms, Ph.D. thesis, University of Washington (2003)
33. J. Migdalek, W. Baylis, J. Phys. B **24**, 99 (1991)
34. M. Sankari, M.V. Suryanarayana, J. Phys. B **31**, 261 (1998)
35. D. Das, S. Barthwal, A. Banerjee, V. Natarajan, Phys. Rev. A **72**, 032506 (2005)
36. C. Kittel, *Introduction to Solid State Physics* (Wiley, New York, 2005)
37. R.A. Holmwood, R. Glang, J. Chem. Eng. Data **10**, 162 (1965)
38. D. Lide, in *CRC Handbook of Chemistry and Physics*, 88th edn. (CRC, Boca Raton, 2007), Chap. 12, p. 200
39. D. Lide, in *CRC Handbook of Chemistry and Physics*, 88th edn. (CRC, Boca Raton, 2007), Chap. 4, p. 136
40. A.S. Bell, P. Gill, H.A. Klein, A.P. Levick, C. Tamm, D. Schnier, Phys. Rev. A **44**, 20 (1991)
41. G. Mainfray, C. Manus, *Multiphoton Ionization of Atoms* (Academic, Toronto, 1984)
42. P. Camus, A. Debarre, C. Morillon, J. Phys. B **13**, 1073 (1980)
43. C. Xu, X. Xu, W. Huang, M. Xue, D. Chen, J. Phys. B **27**, 3905 (1994)
44. W. Demtröder, *Laser Spectroscopy* (Springer, Berlin, 2003)
45. W. Schottky, Phys. Z. **15**, 872 (1914)